SCIENTIFIC REPORTS

OPEN

Dielectric properties of Y and Nb co-doped TiO_2 ceramics

Xianwei Wang[1,2], Bihui Zhang[1,2], Linhai Xu[1,2], Xiaoer Wang[1,2], Yanchun Hu[1,2], Gaohang Shen[1,2] & Lingyun Sun[1,2]

Received: 9 January 2017
Accepted: 24 July 2017
Published online: 17 August 2017

In this work, the $(Y_{0.5}Nb_{0.5})_xTi_{1-x}O_2$ (x = 0.001, 0.01, 0.02, 0.04, 0.06 and 0.1) ceramics (as called YNTO) were fabricated by synthesized through a standard solid-state reaction. As revealed by the X-ray diffraction (XRD) spectra, the YNTOs exhibit tetragonal rutile structure. Meanwhile, the grain size of YNTO ceramics increased and then decreased with the increase of x value, and the largest value reached when x = 0.02. All the YNTO samples display colossal permittivity (~10^2–10^5) over a wide temperature and frequency range. Moreover, the optimal ceramic, $(Y_{0.5}Nb_{0.5})_{0.02}Ti_{0.98}O_2$, exhibits high performance over a broad temperature range from 20 °C to 180 °C; specifically, at 1 kHz, the dielectric constant and dielectric loss are 6.55×10^4 and 0.22 at room temperature, and they are 1.03×10^5 and 0.11 at 180 °C, respectively.

Dielectric materials with colossal permittivity (CP) attract vast research interests due to their great potential applications in wide fields such as device miniaturization and energy storage[1–4]. As typical CP materials, the systems of $BaTiO_3$, $CaCu_3Ti_4O_{12}$ (CCTO), and doped-NiO have been widely explored[5–12]. Unfortunately, $BaTiO_3$ ceramics only show colossal permittivity in a narrow temperature range which is even close to the temperature for phase transition (from ferroelectric to paraelectric phase). Furthermore, the reported work verified that CCTO ceramics display poor stability of their dielectric properties when they were subjected to frequency and temperature variations. Worse still, large dielectric loss and high variation of dielectric constant with temperature impeded the practical application of NiO-based system[6–9,11]. Therefore, huge efforts need to be input in searching for new CP materials which can maintain high dielectric constant and low dielectric loss under a wide range of temperature and frequency.

Previous researches proposed AB co-doped rutile TiO_2 ceramics (A was introduced as an electron-acceptor, such as In^{3+}; B was introduced as an electron-donor, such as Nb^{5+}) as a new sequence of CP materials[1,2,4,13,14]. The existence of a giant dielectric constant ($\varepsilon_r \sim 6 \times 10^4$) along with a low dielectric loss (tan $\delta < 0.02$) at room temperature over varied frequency from 10^2 to 10^6 Hz was found in their research[1]. In fact, Hu *et al.* have illustrated that the In-doping lower the tan δ while Nb ions enhance the ε_r, respectively. The localization of the hopping electrons was found to be near the designated lattice defect states which generate giant defect-diploes; the high-performance in In+Nb co-doped TiO_2 ceramics has been suitably explained by Hu *et al.*[1]. However, Li *et al.* have proposed that conducting grains and resistive grain boundaries are formed in co-doped TiO_2 (In^{3+} and Nb^{5+} doped TiO_2) system, which leads to the internal barrier layer capacitance (IBLC) model. In IBLC model, conducting grains are separated by insulating grain boundaries, which act like capacitors. The CP behavior of materials can be explained on the basis of semiconducting grains and insulating grain boundaries[15–17]. There are other mechanisms used to explain the overall dielectric response in TiO_2-based ceramics, including electron hopping[18] and non-Ohmic sample-electrode contact[3]. In addition, following researches introduced more similar types of ceramics such as Ga+Nb and Al+Nb co-doped TiO_2[2–4,14]. However, both of the Ga+Nb and Al+Nb co-doped rutile TiO_2 ceramics were also reported to show poor dielectric properties compared with the In+Nb co-doped in TiO_2 ceramics[1,3,4,13,16,17,19–21]. Thus, developing more acceptor/donor for the AB co-doped rutile TiO_2 ceramics is essential for pursuing high quality colossal permittivity ceramic materials.

In this study, dielectric materials with the composition of $(Y_{0.5}Nb_{0.5})_xTi_{1-x}O_2$ (x = 0.001–0.1) ceramics were prepared by a conventional solid-state method. The microstructures, dielectric properties, and impedance spectra of these YNTO ceramics were studied, and then we obtained highly temperature and frequency stabilized ceramics $(Y_{0.5}Nb_{0.5})_{0.02}Ti_{0.98}O_2$.

[1]Laboratory of Functional Materials, College of Physics and Materials Science, Henan Normal University, Xinxiang, 453007, China. [2]Henan Key Laboratory of Photovoltaic Materials, Xinxiang, 453007, China. Bihui Zhang, Linhai Xu and Xiaoer Wang contributed equally to this work. Correspondence and requests for materials should be addressed to X.W. (email: xwwang2000@163.com)

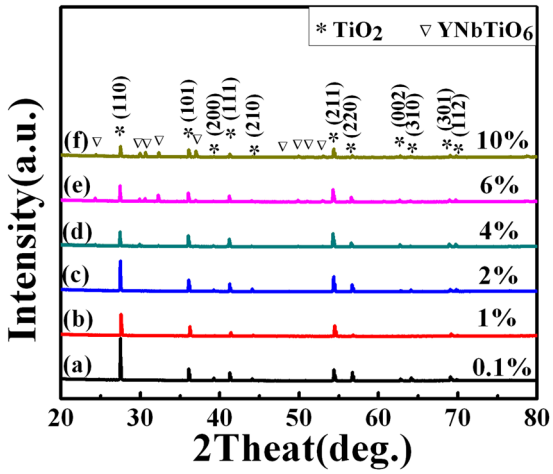

Figure 1. Determination of the phase structure for YNTO ceramics. (**a**)–(**f**) XRD spectra of $(Y_{0.5}Nb_{0.5})_xTi_{1-x}O_2$ when x = 0.001, 0.01, 0.02, 0.04, 0.06 and 0.1.

Composition	Lattice parameter a(Å)	Lattice parameter c(Å)	Densities Therotical g/cm³	Densities Measured	Relative density
$(Y_{0.5}Nb_{0.5})_{0.001}Ti_{0.999}O_2$	4.588	2.954	4.27	3.89	91.10
$(Y_{0.5}Nb_{0.5})_{0.01}Ti_{0.99}O_2$	4.589	2.954	4.29	3.93	91.61
$(Y_{0.5}Nb_{0.5})_{0.02}Ti_{0.98}O_2$	4.591	2.956	4.30	3.94	91.63
$(Y_{0.5}Nb_{0.5})_{0.04}Ti_{0.96}O_2$	4.598	2.959	4.33	4.38	91.22
$(Y_{0.5}Nb_{0.5})_{0.06}Ti_{0.94}O_2$	4.598	2.958	4.38	3.99	91.10
$(Y_{0.5}Nb_{0.5})_{0.10}Ti_{0.90}O_2$	4.596	2.949	4.49	4.06	90.42

Table 1. Crystal parameters of YNTO ceramics. Crystal parameters of $(Y_{0.5}Nb_{0.5})_xTi_{1-x}O_2$ ceramics when x = 0.001, 0.01, 0.02, 0.04, 0.06 and 0.1.

Results and Discussion

XRD spectrums of all sintered YNTO ceramics with different co-doping concentrations are plotted together for comparison in Fig. 1. All the YNTO ceramics show pure tetragonal rutile TiO_2 (JCPDS 21–1276) phase when x varies from 0.001 to 0.02. However, when the quantity x is further increased to 0.04, the secondary phase of $YNbTiO_6$ starts to show up and is detected in 0.04, 0.06 and 0.1 samples due to the phase transformation caused by the excessive Y^{3+} and Nb^{5+} co-doping into the TiO_2 lattice, Moreover, both the a and c values of all YNTO ceramics are comparable to those reported in the literature for the In+Nb co-doped ceramics[20]. For clearer comparison, the lattice parameters of YNTO ceramics are listed in Table 1. According to Table 1, the cell volume expands (the a and c parameters increase) when x varies from 0.001 to 0.02, as is resulted from the substitution of small Ti^{4+} (ionic radius = 60.5 pm) by the larger Nb^{5+} (ionic radius = 64 pm) and Y^{3+} (ionic radius = 90 pm) in the TiO_2 lattice. When the quantity x is further increased to 0.04, 0.06 and 0.1, the lattice parameters of the co-doped ceramics show an abnormal tendency that can be attributed to the formation of an impurity phase.

SEM images reveal that the grain sizes of all the sintered YNTO ceramics increase and then decrease versus x in Fig. 2. The grain size of all YNTO ceramics reaches the largest value when x = 0.02, which is consistent with Nb, In and Al, Sb co-doped TiO_2 ceramics[1,22]. For 0.04 sample, the EDS results of the as pointed region confirm the elemental ratio of Y:Nb:Ti is close to 1:1:1 (Y: Nb: Ti = 6.2:7.73:7.09), which is in accordance with the XRD results for the $YNbTiO_6$ phase (the elemental ratio in another zone is also close to 1:1:1, as is shown in Fig. S1). In addition, when further enlarge the co-doping ratio of Y and Nb over 0.04, the grain boundaries start to restrain instead of expanding which should be ascribed to the formation of secondary phase, leading to the retardation of grain growth. As shown in Table 1, the relative densities increase to the maximum value at x = 0.02 and then decrease when co-doping ratio over 0.04, which is commensurate with the XRD and SEM data, demonstrating the solidifying benefit from the Y and Nb co-doping. Therefore, the Y and Nb co-doping profit the YNTO ceramics in enlarged cell volume, broadened grain boundary and more compact density, which would theoretically enhance the dielectric properties. To figure out this prediction, the stabilities of dielectric constant and loss are tested versus a wide range of temperature (20 to 180 °C) and frequency (10^2–10^6 Hz).

In general, all the co-doped YNTO ceramics exhibit relatively higher dielectric constant than the pure TiO_2, except for the co-doping as low as 0.001 which shows comparable ε_r with the pristine[15]. The YNTO ceramics show the similar behavior of dielectric constant change versus frequency at room temperature, i.e. the value of ε_r drops with the increase of frequency, as shown in Fig. 3(a). The observed high dielectric constant in the low-frequency range is caused by the space polarization as was also demonstrated in the NiO-based system[6].

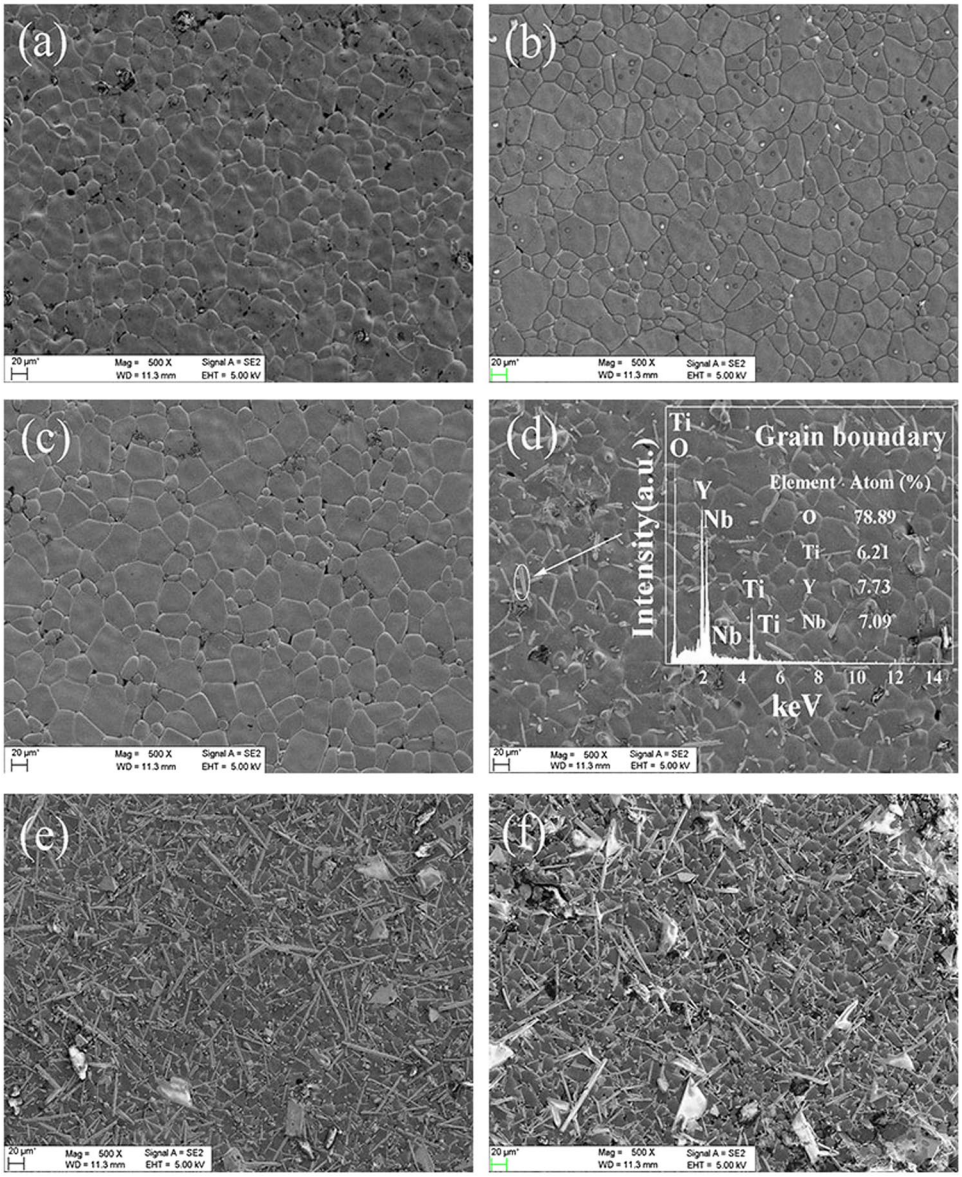

Figure 2. The SEM images for YNTO ceramics. (**a**)–(**f**) SEM images of $(Y_{0.5}Nb_{0.5})_xTi_{1-x}O_2$ when x = 0.001, 0.01, 0.02, 0.04, 0.06 and 0.1; the inset in (**d**) shows the energy dispersion spectrum of pointed region when x = 0.04.

Fortunately, the dielectric constant increases by several magnitudes when the co-doping concentration is higher than 0.01. Regarding the co-doping content, 0.01 and 0.1 reach the similar enhancement effect indicating the negative effect of excessive co-doping. While 0.02, 0.04 and 0.06 co-doping boost the dielectric constant to almost two orders higher than 0.01 and 0.1, demonstrating the proper amount of Y and Nb co-doping region. The optimal co-doping level is determined to be 0.02, where the YNTO composite remain a rather stable and high dielectric constant ($\varepsilon_r \sim 6.55 \times 10^4$ at 1 kHz) over a wide frequency range from 10^2 Hz to 10^6 Hz. Unfortunately, this enhancement disappears when co-doping concentration is further increased over 0.04 where secondary phase starts to form as was verified in the XRD spectrum analysis. Hence, the secondary phase formation will decrease the dielectric constant. Though the highest ε_r value ($\sim 2.58 \times 10^5$ at 1 kHz) is obtained for the YNTO ceramic when x = 0.04, it decreases quickly with the increasing of frequency, which is unsatisfying. Another important parameter for dielectric property is the dielectric loss along with frequency increase. As shown in Fig. 3(b), the curve of tan δ versus frequency shows a dissipation peak, and the increase of dielectric loss at low frequency might due to the direct current conduction. Meanwhile, the dielectric loss varies with x content, and the lowest value at 1 kHz is observed in $(Y_{0.5}Nb_{0.5})_{0.02}Ti_{0.98}O_2$ (tan δ = 0.29, 0.46, 0.22, 0.62, 0.38 and 0.31 when x = 0.001, 0.01, 0.02, 0.04, 0.06 and 0.1, respectively). Furthermore, both the 0.02 and 0.06 co-doped YNTO ceramics exhibit quite stable dielectric loss under the entire tested frequency range while the 0.02 co-doped ceramic exhibits relatively lower tan δ value.

To figure out the stability of the optimized $(Y_{0.5}Nb_{0.5})_{0.02}Ti_{0.98}O_2$ ceramic as a function of frequency at different temperatures, its dielectric constant (Fig. 4(a)) and dielectric loss (Fig. 4(b)) are examined from 20 °C to 180 °C.

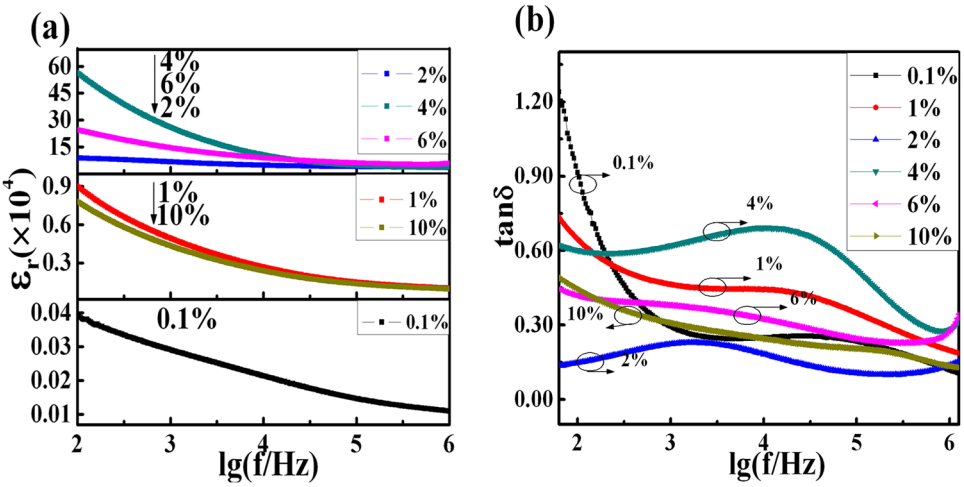

Figure 3. The dielectric behavior of YNTO ceramics. The effects of frequency on (**a**) dielectric constant and (**b**) dielectric loss at room temperature.

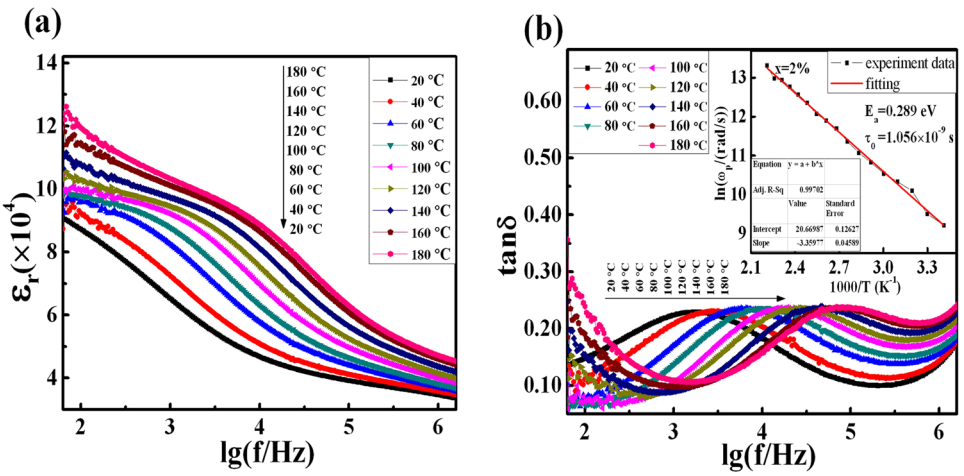

Figure 4. The dielectric behavior of YNTO ceramics. The effects of frequency on (**a**) dielectric constant and (**b**) dielectric loss of $(Y_{0.5}Nb_{0.5})_{0.02}Ti_{0.98}O_2$ sample under divergent temperatures; the inset in (**b**) shows the Arrhenius fitting plot of the tan δ relaxation values.

The overall value of ε_r is above 10^4 and it enlarges rapidly as a function of temperature, which can be attributed to the rise of conductivity at higher temperature[5,21,23,24]. The existence of the plateau of the dielectric constant at low-frequency range demonstrates a high frequency-independence property in accordance with previous analysis. Then, the dielectric constant decreases to another plateau at higher frequencies. The increasing of dielectric constant as a function of temperature could lead to the variation of dielectric loss. Regarding the dielectric loss, the dissipation peak appears at medium frequency range (~10^3–10^5 Hz) with the highest value which is typical for CP co-doped ceramics[10,17]. The relaxation peak could be fitted well with Debye relaxation model, as shown in Fig. S2. Additionally, Fig. 4(b) depicts that there should be a dissipation peak shifting to higher frequency with the increasing of temperature, which is in correspondence to the Debye relaxation[1,3,9,25–27]. The dielectric relaxation time (τ) could be calculated with the extreme value relation

$$\ln(\omega_p\tau) = 0, \tag{1}$$

where circular frequency ω_p equals to $2\pi f_p$ and f_p is the characteristic frequency at the peak of tan δ. The fast increase of f_p indicates the decrease of τ with temperature increase, which is due to the thermally excited relaxation process[1,3,7,24]. The activation energies required for these relaxations can be calculated with the Arrhenius law as

$$\tau = \tau_0 \exp\left(\frac{E_a}{K_B T}\right), \tag{2}$$

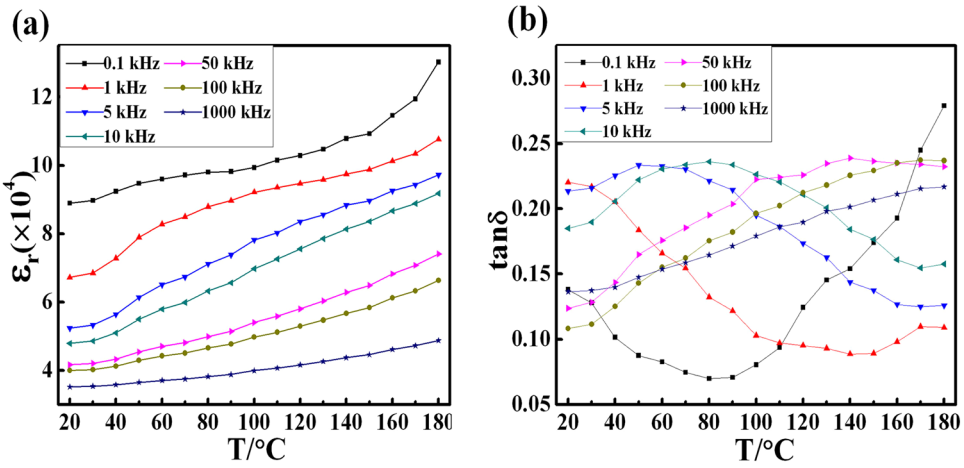

Figure 5. The dielectric behavior of YNTO ceramics. The effects of temperature on (**a**) dielectric constant and (**b**) dielectric loss of $(Y_{0.5}Nb_{0.5})_{0.02}Ti_{0.98}O_2$ sample under varied frequencies.

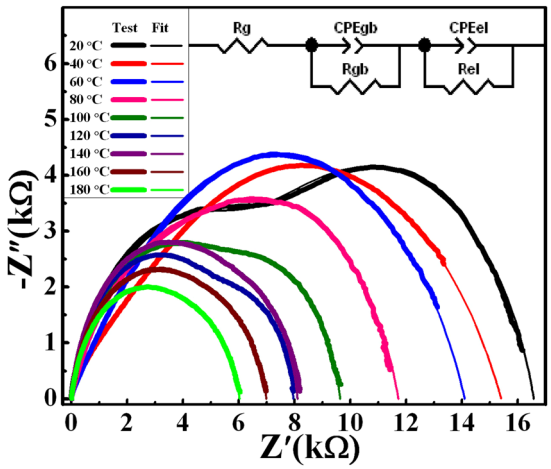

Figure 6. Impedance spectra for $(Y_{0.5}Nb_{0.5})_{0.02}Ti_{0.98}O_2$ ceramic at different temperatures.

where τ_0 is the pre-exponential factor, E_a is the activation energy for the relaxation, K_B is the Boltzmann constant, and T is the temperature corresponding to the peak of tan δ. So the equation (2) can be derived as

$$\ln\omega_p = -\frac{E_a}{K_B T} - \ln\tau_0 \tag{3}$$

A linear regression of $\ln(\omega_p)$ versus 1/T fits the data quite well, as is shown in the inset of Fig. 4(b), indicating a non-polaron type relaxation all YNTO ceramics due to a hopping motion of localized carriers[21]. The values of τ_0 and E_a are calculated to be 1.056×10^{-9} s and 0.289 eV, and the value of E_a is close to the activation energies for Nb-doped rutile TiO_2[15]. Thus the dielectric properties of the Y and Nb co-doped TiO_2 ceramics possess high temperature stability.

To better understand the stability of dielectric constant and dielectric loss as a function of temperature at different frequencies, the values of ε_r and tan δ of x = 0.02 are plotted in Fig. 5. It can be seen that the ε_r value increases slightly with temperature increase, indicating the high dielectric constant of Y and Nb co-doped TiO_2 ceramics over a broad temperature range. As was detected in previous test, a broad peak of tan δ appears due to the Debye relaxor behavior. And the dielectric relaxation time would decrease with the increasing of temperature.

Figure 6 presents the impedance spectra of the $(Y_{0.5}Nb_{0.5})_{0.02}Ti_{0.98}O_2$ sample as a function of temperature range from 20 °C to 180 °C in the frequency range of 40 Hz–10 MHz. In particular, the impedance spectra could be fitted with an appropriate equivalent circuit, as shown in the inset of Fig. 6. R_g, R_{gb} and R_{el} are the resistance of grain, grain boundary and electrode, respectively, and CPE_{gb} and CPE_{el} is constant phase element of grain boundary and electrode, respectively. The nonzero intercept on the Z′ axis is observed at different temperatures, and it is corresponding to the grain response. The grain resistance (R_g) values of 0.02 sample at different temperatures are ≈1–15 Ω, which are comparable to those reported in the literature[17]. In addition, the R_g value increases slightly with temperature, indicating that grains show conductive behavior in 0.02 sample, which is also reported in

other reports[16,17]. The left part of the arc at medium frequency corresponds to grain boundary response, and the R_{gb} decreases gradually as a function of temperature. Right part of arc at low frequency is associated with the electrode response, and the low-frequency intercept in that case gives the resistance of electrode. According to the analysis of the impedance spectrum measured at 180 °C, R_g, R_{gb}, R_{el} is about 15 Ω, 2938 Ω, and 6017 Ω, respectively. In other words, the premise of the IBLC effect ($R_{gb} \gg R_g$) is successfully established, indicating that the samples exhibit electrical inhomogeneous configuration. Based on the above discussion, the CP behavior in Y+Nb co-doped ceramic could be explained by IBLC model associated with conducting grains and insulating grain boundaries, where the electrons can move smoothly inside grains, but were accumulated in grain boundaries. Which is consistent with the prior literature[13,15–17], the Y and Nb co-doping in TiO_2 ceramics enhance their dielectric properties due to the IBLC model. These satisfying results fulfill our design strategy and pave to way for more electron acceptor/donor co-doping ceramics.

In summary, $(Y_{0.5}Nb_{0.5})_xTi_{1-x}O_2$ ceramics (x = 0.001, 0.01, 0.02, 0.04, 0.06 and 0.1) were obtained and their morphology and crystal structures are well examined with SEM and XRD characterizations, and the co-doping of Y+Nb resulted in an expansion of lattice parameters (the a and c values). This scarcely reported series of ceramics show stable dielectric properties even at high temperature of 180 °C. After careful tuning of the x value in $(Y_{0.5}Nb_{0.5})_xTi_{1-x}O_2$ ceramics, the optimal ceramic of $(Y_{0.5}Nb_{0.5})_{0.02}Ti_{0.98}O_2$ is realized with a high value of ε_r (~6.55×10^4) and relative low value of tan δ (~0.22). Additionally, the existence of CP behavior in sample had been explained by an internal barrier layer capacitance (IBLC) model, which consists of conducting grains and insulating grain boundaries.

Methods

Sample preparation. TiO_2 (purity: 99.99%), Nb_2O_5 (purity: 99.9%) and Y_2O_3 (purity: 99.99%) were used as raw materials. The TiO_2 and Nb_2O_5 were heated to dry at 200 °C for 12 h; and Y_2O_3 was heated at 800 °C for 2 h to decompose any carbonate. After heat treatment, the source materials were weighed immediately for subsequent weight determination. The synthesis of $(Y_{0.5}Nb_{0.5})_xTi_{1-x}O_2$ (x = 0.001, 0.01, 0.02, 0.04, 0.06, 0.1) was conducted via a standard solid-state reaction method. First, the treated raw materials were mixed by ball milling in ethanol with ZrO_2 as the medium for 10 h at 580 r/min. Second, the mixture was evaporated at 80 °C to remove the ethanol residue. Third, the resulting powder was calcined at 1100 °C for 10 h, and ground with polyvinyl acetate (PVA) solutions (5 wt. %) in an agate mortar. Finally, the resultant powder was pressed into cylindrical pellets under a pressure of 250 MPa for 5 minutes; then the pellets were sintered at 1500 °C for 10 h.

Characterization. The crystal structures of the YNTO ceramics were identified by X-ray diffraction (XRD, Bruker D8 discover) at 40 kV and 40 mA. And their microstructures were characterized via a Field-emission scanning electron microscope (FE-SEM, Zeiss SUPRA 40). Both sides of the YNTO ceramics were coated with silver paste and heated at 650 °C to form silver electrodes; then the dielectric properties and impedance spectroscopic were determined by a precision impedance analyzer (HP, 4294 A). Moreover, the stabilities of dielectric properties for the $(Y_{0.5}Nb_{0.5})_{0.02}Ti_{0.98}O_2$ ceramic were tested in the temperature range of 20–180 °C.

References

1. Hu, W. *et al*. Electron-pinned defect-dipoles for high-performance colossal permittivity materials. *Nat. Mater.* **12**, 821–826 (2013).
2. Li, Z., Wu, J., Xiao, D., Zhu, J. & Wu, W. Colossal permittivity in titanium dioxide ceramics modified by tantalum and trivalent elements. *Acta Mater.* **103**, 243–251 (2016).
3. Dong, W. *et al*. Colossal dielectric behavior of Ga plus Nb co-doped rutile TiO_2. *ACS Appl. Mater. Interfaces* **7**, 25321–25325 (2015).
4. Hu, W. *et al*. Colossal dielectric permittivity in (Nb plus Al) codoped rutile TiO_2 ceramics: compositional gradient and local structure. *Chem. Mater.* **27**, 4934–4942 (2015).
5. Wang, J. Q., Huang, X., Zheng, X. H. & Tang, D. P. Structure and electric properties of $CaCu_3Ti_4O_{12}$ ceramics prepared by rapid sintering. *J. Mater. Sci. - Mater. Electron.* **27**, 1345–1349 (2016).
6. Khemprasit, J. & Khumpaitool, B. Influence of Cr doping on structure and dielectric properties of $Li_xCr_yNi_{1-x-y}O$ ceramics. *Ceram. Int.* **41**, 663–669 (2015).
7. Manna, S. & De, S. K. Giant dielectric permittivity observed in Li and Zr co-doped NiO. *Solid State Commun.* **150**, 399–404 (2010).
8. Maensiri, S., Thongbai, P. & Yamwong, T. Giant dielectric response in (Li, Ti)-doped NiO ceramics synthesized by the polymerized complex method. *Acta Mater.* **55**, 2851–2861 (2007).
9. Pongha, S., Thongbai, P., Yamwong, T. & Maensiri, S. Giant dielectric response and polarization relaxation mechanism in (Li,V)-doped NiO ceramics. *Scripta Mater.* **60**, 870–873 (2009).
10. Sun, L. *et al*. Sol-gel synthesized pure $CaCu_3Ti_4O_{12}$ with very low dielectric loss and high dielectric constant. *Ceram. Int.* **41**, 13486–13492 (2015).
11. Khumpaitool, B. & Khemprasit, J. Improvement in dielectric properties of Al_2O_3-doped $Li_{0.30}Cr_{0.02}Ni_{0.68}O$ ceramics. *Mater. Lett.* **65**, 1053–1056 (2011).
12. Wang, X. W. *et al*. Calcining temperature dependence on structure and dielectric properties of $CaCu_3Ti_4O_{12}$ ceramics. *J. Mater. Sci.-Mater. Electron.* **27**, 12134–12140 (2016).
13. Li, J. L. *et al*. Evidences of grain boundary capacitance effect on the colossal dielectric permittivity in (Nb plus In) co-doped TiO_2 ceramics. *Sci. Rep.* **5**, 8295 (2015).
14. Cheng, X. J., Li, Z. W. & Wu, J. G. Colossal permittivity in ceramics of TiO_2 co-doped with niobium and trivalent cation. *J. Mater. Chem. A* **3**, 5805–5810 (2015).
15. Mandal, B. P. *et al*. Enhancement of dielectric constant in a niobium doped titania system: an experimental and theoretical study. *New J. Chem.* **40**, 9526–9536 (2016).
16. Li, J. *et al*. Microstructure and dielectric properties of (Nb plus In) co-doped rutile TiO_2 ceramics. *J. Appl. Phys.* **116**, 074105 (2014).
17. Wu, Y. Q., Zhao, X., Zhang, J. L., Su, W. B. & Liu, J. Huge low-frequency dielectric response of (Nb, In)-doped TiO_2 ceramics. *Appl. Phys. Lett.* **107**, 217601 (2015).
18. Zhao, X. G. *et al*. Origin of colossal permittivity in $(In_{1/2}Nb_{1/2})TiO_2$ via broadband dielectric spectroscopy. *PCCP* **17**, 23132–23139 (2015).
19. Gai, Z. G. *et al*. A colossal dielectric constant of an amorphous TiO_2: (Nb, In) film with low loss fabrication at room temperature. *J. Mater. Chem. C* **2**, 6790–6795 (2014).
20. Li, J. L., Li, F., Xu, Z., Zhuang, Y. Y. & Zhang, S. J. Nonlinear I-V behavior in colossal permittivity ceramic: (Nb plus In) co-doped rutile TiO_2. *Ceram. Int.* **41**, S798–S803 (2015).

21. Tuichai, W., Danwittayakul, S., Maensiri, S. & Thongbai, P. Investigation on temperature stability performance of giant permittivity (In plus Nb) in co-doped TiO_2 ceramic: a crucial aspect for practical electronic applications. *RSC Adv.* **6**, 5582–5589 (2016).
22. Tuichai, W., Srepusharawoot, P., Swatsitang, E., Danwittayakul, S. & Thongbai, P. Giant dielectric permittivity and electronic structure in (Al plus Sb) co-doped TiO_2 ceramics. *Microelectron. Eng.* **146**, 32–37 (2015).
23. Liu, X. Q., Wu, Y. J., Chen, X. M. & Zhu, H. Y. Temperature-stable giant dielectric response in orthorhombic samarium strontium nickelate ceramics. *J. Appl. Phys.* **105**, 054104 (2009).
24. Wu, J., Nan, C. W., Lin, Y. & Deng, Y. Giant dielectric permittivity observed in Li and Ti doped NiO. *Phys. Rev. Lett.* **89**, 1662–1666 (2002).
25. Fu, J. Y. On the theory of the universal dielectric relaxation. *Philos. Mag.* **94**, 1788–1815 (2014).
26. Wang, C. C. *et al*. Dielectric relaxations in rutile TiO_2. *J. Am. Ceram. Soc.* **98**, 148–153 (2015).
27. Thongbai, P., Yamwong, T. & Maensiri, S. Effects of Li and Fe doping on dielectric relaxation behavior in (Li, Fe)-doped NiO ceramics. *Mater. Chem. Phys.* **123**, 56–61 (2010).

Acknowledgements

This work has been supported by the National Natural Science Foundation of China (No. 51402091, No. 51601059, No. 11304082 and No. 11404102), the scientific research foundation for new newly graduated PhD students in Henan Normal University (No. 11114), and the National University Student Innovation Program.

Author Contributions

X.W.W. and Y.C.H. conceived and designed the experiments. B.H.Z., L.H.X. and X.E.W. assisted in the preparation of crystal sample and the measurement of dielectric property. X.E.W. and L.Y.S. assisted in the measurement of SEM. X.W.W., B.H.Z. and L.H.X. analyzed the data and prepared the manuscript. All authors discussed the results and contributed to the refinement of the manuscript.

Additional Information

Supplementary information accompanies this paper at doi:10.1038/s41598-017-09141-0

Competing Interests: The authors declare that they have no competing interests.

Publisher's note: Springer Nature remains neutral with regard to jurisdictional claims in published maps and institutional affiliations.